Egyptian Journal of Petroleum (2013) **22**, 451–470

Egyptian Petroleum Research Institute

Egyptian Journal of Petroleum

www.elsevier.com/locate/egyjp
www.sciencedirect.com

FULL LENGTH ARTICLE

A study of the corrosion inhibition of mild steel C1018 in CO_2-saturated brine using some novel surfactants based on corn oil

V.M. Abbasov [a], Hany M. Abd El-Lateef [a,b,*], L.I. Aliyeva [a], E.E. Qasimov [a], I.T. Ismayilov [a], Mai M. Khalaf [a,b]

[a] *Mamedaliev Institute of Petrochemical Processes, National Academy of Sciences of Azerbaijan, AZ1025 Baku, Azerbaijan*
[b] *Chemistry Department, Faculty of Science, Sohag University, 82524 Sohag, Egypt*

Received 20 December 2012; accepted 19 February 2013
Available online 8 December 2013

KEYWORDS

Mild steel;
Surfactants;
Corn oil;
Corrosion inhibition;
Langmuir isotherm;
SEM

Abstract The influence of the concentration of novel surfactants based on corn oil on the corrosion behavior of carbon steel in CO_2 saturated solution at different temperatures was studied. The investigation involved weight loss, LPR corrosion rate and extrapolation of cathodic and anodic Tafel lines method. Results obtained show that the surfactants studied are efficient corrosion inhibitors for carbon steel in CO_2 saturated brine. The inhibition efficiency (*IE*%) increases with an increase in the concentration of the studied surfactant. The inhibition process was attributed to the formation of the adsorbed film on the metal surface that protects the surface against the corrosive agent. The data exhibited that the inhibition efficiency slightly increases with increasing temperature. The surface activity of the synthesized surfactant solutions was determined using surface tension measurements at 25 °C. Adsorption of inhibitors was found to obey the Langmuir isotherm. The standard enthalpy, $\Delta H^{\circ}_{ads.}$, entropy, $\Delta S^{\circ}_{ads.}$ and free energy changes of adsorption were evaluated; the calculated values of $\Delta H^{\circ}_{ads.}$ and ΔG°_{ads} were negative while those for $\Delta S^{\circ}_{ads.}$ were positive. Mainly, all the above results are suggestive of chemisorption of the surfactant molecules on the metal surface. Scanning electron microscopy (SEM) and Energy dispersive X-ray fluorescence (EDRF) observations of the electrode surface confirmed the existence of such an adsorbed film.

1. Introduction

Mild steel alloys are the most commonly used construction materials for pipelines in the oil and gas industry but they are very susceptible to both a high general corrosion rate and severe localized corrosion [1]. CO_2 corrosion is one of the most significant causes in the oil and gas pipeline failures and occurs at all stages of production from downhole to

* Corresponding author at: Chemistry Department, Faculty of Science, Sohag University, 82524 Sohag, Egypt.
E-mail address: Hany_shubra@yahoo.co.uk (H.M. Abd El-Lateef).
Peer review under responsibility of Egyptian Petroleum Research Institute.

ELSEVIER Production and hosting by Elsevier

1110-0621 © 2013 Production and hosting by Elsevier B.V. on behalf of Egyptian Petroleum Research Institute.
Open access under CC BY-NC-ND license. http://dx.doi.org/10.1016/j.ejpe.2013.11.002

surface equipment and processing facilities [2,3]. Carbon dioxide gas dissolves into saltwater and forms weak carbonic acid. This acid reacts with the iron of the steel pipes enhancing their corrosion rate. Although mild steel corrosion resistance is poor in aggressive environments, it is usually the most cost effective option with the use of organic corrosion inhibitors. Commercial corrosion inhibitors consist of at least one of the following surfactants: fatty acids, amines, fatty amines/diamines, fatty amido/amines or imidazolines, quaternary amines, other amine derivates, and oxygen, sulfur or phosphorous containing compounds [4].

Specific types of organic inhibitors are represented by surfactants [5–15]. Surfactant molecules consist of nonpolar hydrophobic and polar hydrophilic groups [16]. Surfactant inhibitors have many advantages, for example, high inhibition efficiency, low price, low toxicity, and easy production [17,18]. Moreover, the investigation of surfactants adsorbed on metal surfaces is extremely important in electrochemical studies such as corrosion inhibition, adhesion, lubrication, and detergency [19]. Surfactants are widely employed in the petroleum industry to protect iron and steel equipments used in drilling, production, transport, and refining of hydrocarbons [20]. The efficiency of the inhibited film depends on the inhibitor concentration and contact time with the metal surface.

It is generally accepted that organic molecules inhibit corrosion via adsorption at the metal–solution interface [21,22]. Two primary mechanisms of adsorption are associated with organic compounds: they act by blocking the reaction sites or generating a physical barrier to reduce the diffusion of corrosive species to the metal surface. The mode of adsorption is dependent on the following factors: chemical and electronic structure of the molecule, inhibitor concentration, solution chemistry, nature and surface charge of the metal surface, electrochemical potential at the interface and the temperature of the corrosion reaction [23].

The type of corrosion caused by dissolved CO_2 varies considerably depending on the changes of the precise environmental conditions (temperature, pH, partial pressure of CO_2, etc.). Temperature is the most important influencing factor in CO_2 corrosion environments. In general, temperature has a great effect on the rate of metal corrosion [24] and its variation is a very useful tool for studying and clarifying the adsorption mechanism of an inhibitor. It is well known that the effect of temperature is highly complex but it provides the possibility of calculating the thermodynamic adsorption and kinetic corrosion parameters, which helps in determining the type of adsorption of the studied inhibitor.

In the present work, we describe the synthesis and characterization of novel surfactants based on corn oil. Corrosion inhibition of mild steel C1018 in CO_2-saturated 1% NaCl solution in the presence of synthesized surfactants has been studied by using weight loss, LPR corrosion rate, extrapolation of cathodic and anodic Tafel lines and surface tension techniques complemented with some SEM and EDRF observations. Also this work was purposed to test the experimental data obtained from the extrapolation of cathodic and anodic Tafel lines method with several adsorption isotherms at different temperatures, in order to determine the thermodynamic functions for the adsorption process and get more information on the mode of adsorption.

2. Materials and methods

2.1. Chemical composition of the investigated mild steel C1018

Electrodes are made of steel grade 080A15 and have an area of 4.55 cm^2 (rotating cylinder electrode). These electrodes are used for one time. The mechanical properties of the mild steel measured at room temperature were provided by the supplier and shown as follows: tensile strength equal to 490 MPa and elongation to failure equal to 16%. The chemical composition of mild steel used in this study was given in Table 1. The data were provided by the European Corrosion Supplies Ltd.

2.2. Synthesis of the inhibitors

The inhibitors were synthesized in our laboratory based on corn oil. The corn oil is a mixture of different fatty acids as shown in Table 2. The corn oil was hydrolyzed with a solution of 25% NaOH for 7 h at 90 °C. This process produced the sodium salt of fatty acid, was reacted with 37% HCl acid solution to liberate the free hydrolyzed fatty acid. Based on the prepared fatty acid the sulfating syntheses were performed. The product is sulfated fatty acid. The product was characterized by FT-IR spectroscopy using a model FT-IR, Spectrum BX spectrometer using KBr disks and physical–chemical methods (Table 3).

Five types from surfactants were synthesized in high purity by the following compositions: [R-CH-(OSO_3X)-$COOX$] (where $X = Na,\ K,\ NH_4$, $–NH–CH_2–CH_2–OH$ and $–N–(CH_2–CH_2–OH)_2$). Sulfated fatty acid was taken at a molar ratio 1:2 with mono and diethanolamine. The components of reactions were mixed well for a period 2 h at 50 °C to produce monoethanolamine and diethanolamine sulfated fatty acid. The structures and code numbers of the synthesized surfactants are shown in Table 4. The freezing temperature of synthesized surfactants was measured and listed in Table 4.

2.3. Preparation of solutions

The aggressive solution, 1% NaCl solution, was prepared by dissolving of analytical grade NaCl in distilled water. The concentration range of the prepared surfactants was from 10 to 100 ppm by mole used for corrosion measurements. All inhibitor solutions were prepared using a mixture of distilled water and isopropyl alcohol in a ratio 70:30.

2.4. Corrosion measurements

The measurements were performed on the rotating cylinder electrode (A = 4.55 cm^2). This electrode was used for one time. The reference electrode was a saturated calomel electrode (SCE) to which all potentials are referred.

Before beginning the experiment, the prepared 1% – of sodium chloride solution was stirred by a magnetic stirrer for 30 min in a 1000 ml cell. Then this cell was thermostated at a temperature range 20–50 °C for 1 h under a pressure of 0.9 bar. The solution was saturated with carbon dioxide. To remove any surface contamination and air formed oxide, the working electrode was kept at −1500 mV (SCE) for 5 min in the tested solution, disconnected and shaken free of adsorbed

Table 1 Chemical composition of mild steel C1018.

Element	Si	Ni	Cr	S	C	P	Mn	Fe
Content, (wt.%)	0.37	0.01	0.07	0.03	0.18	0.03	0.71	Balance

Table 2 The composition of corn oil (Percent by weight of total fatty acids).

Fatty acid		Composition (%)
Saturated	Palmitic acid	11
	Stearic acid	2
Mono unsaturated	Oleic acid	28
Poly unsaturated	Linolenic acid	58
	Alpha linolenic acid	1

hydrogen bubbles and then cathodic and anodic polarizations were recorded. ACM Gill AC instrument connected with a personal computer was used for the measurements.

2.4.1. The extrapolation of cathodic and anodic Tafel lines

The extrapolation of cathodic and anodic Tafel lines was carried out in a potential range ± 200 mV with respect to corrosion potential (E_{corr}) at a scan rate of 1 mV/s.

2.4.2. Linear polarization resistance corrosion rate

The linear polarization resistance (LPR) corrosion rate bubble-test method involves evaluating the corrosion of steel in simulated brine saturated with CO_2 at a temperature equivalent to that in the field. The LPR method is ideal for plant monitoring offering an almost instantaneous indication of the corrosion rate, allowing for quick evaluation of remedial action and minimizing unscheduled downtime. The potential of the working electrode was varied by a CoreRunning programme (Version 5.1.3.) through an ACM instrument Gill AC. The CoreRunning programme converts a corrosion current in mA/cm^2 to a corrosion rate in mm/year. A cylindrical mild steel rod of the composition 080A15 GRADE STEEL was used as a working electrode. Gill AC technology allows measure DC and AC signals using standard Sequencer software. A small sweep from typically -10 to $+10$ mV at 10 mV/min around the rest potential is performed.

Table 3 Physical and chemical properties of fatty acid and sulfated fatty acid synthesized based on corn oil.

Acid	Acid number (mg KOH/g)	Molecular weight (g/mol)	Iodine number 100 g iodine/g of sample	Density, d_4^{20} (kg/m^3)	Refraction, $\eta_2 0^D$
Fatty acid	147.5	278	46	911	1.4660
Sulfated fatty acid	284	376	–	917	1.4580

Table 4 List of the synthesized surfactants includes, code number, name and structure.

Code number of the surfactants	Name and abbreviation	Structure	Molecular weight (g /mol)	Freezing temperature (°C)
I	Sodium salt of sulfated fatty acid (SSFA)	R-(CH$_2$)$_7$-CH(O—SO$_3$Na)-(CH$_2$)$_7$-COONa	420	−19
II	Potassium salt of sulfated fatty acid (PSFA)	R-(CH$_2$)$_7$-CH(O—SO$_3$K)-(CH$_2$)$_7$-COOK	452	−24
III	Ammonium salt of sulfated fatty acid (ASFA)	R-(CH$_2$)$_7$-CH(O—SO$_3$NH$_4$)-(CH$_2$)$_7$-COONH$_4$	410	−23
IV	Monoethanolamine sulfated fatty acid(MSFA)	R-(CH$_2$)$_7$-CH(O—SO$_2$-NH-CH$_2$-CH$_2$-OH)-(CH$_2$)$_7$-CO-NH-CH$_2$-CH$_2$-OH	462	−21
V	Diethanolamine sulfated fatty acid (DSFA)	R-(CH$_2$)$_7$-CH(O—SO$_2$-N(CH$_2$-CH$_2$-OH)$_2$)-(CH$_2$)$_7$-CO-N(CH$_2$-CH$_2$-OH)$_2$	551	−20

2.4.3. Weight loss measurements

Corrosion inhibition tests were performed using mild steel specimens. These specimens were washed with deionized water, degreased with absolute ethanol. The specimens were dried and kept in a desiccator. The weight loss (in mg cm^{-2} d^{-1}) was determined at different immersion times by weighing the cleaned samples before and after hanging the specimens into 1000 cm^3 of the corrosive solution, namely 1% NaCl saturated with CO_2 in a closed beaker with stirring in the absence and presence of various concentrations of the investigated surfactant. Triplicate specimens were exposed to each condition and the mean weight loss was reported.

Each experiment was performed with freshly prepared solution. Measurements were conducted at a temperature range of 20–50 °C for the investigated NaCl solution. For this purpose, Magnetic Stirrer with Heater (115 V, 50/60 Hz) was used. The test conditions are summarized in Table 5.

2.4.4. Surface tension measurements

It is of interest to study the micellar properties of solutions of these compounds in order to correlate their surface active properties with critical micelle concentration (CMC). The surface tensions were determined by DuNouy Tensiometer, Kruss Type 8451 and the temperature was maintained precisely at 25 °C. Critical micelle concentration (CMC) values of surfactants were determined, according to the break points in the plots of the surface tension versus ln molar concentration of the investigated surfactants.

2.5. Surface characterization

In order to observe any changes in surface morphologies of the mild steel samples after testing, the specimens were first immersed in the test media with and without an inhibitor for 6 days, then cleaned with bi-distilled water and acetone, and dried with cool air. Then the morphology of the tested sample was observed by using HORIBA XGT-7000 – Energy dispersive X-ray fluorescence (EDRF) connected with scanning electron microscope (SEM). The tested samples obtained from weight loss measurements were used in investigations.

2.6. Thermal analyses

The thermal behavior of inhibitor **I** was studied by thermogravimetric (TG) and differential scanning calorimetry (DSC) methods at a temperature interval of 20–600 °C with a heating rate of 10 K/min in a corundum pan with sample weighting 10.0 ± 0.1 mg in a flow (40 ml/min) of nitrogen gas by using Simultaneous TG–DTA/DSC Apparatus "STA 449 F3 Jupiter".

2.7. Methods of evaluation of corrosion parameters

Steady state of open circuit corrosion potential (E_{corr}) for the investigated electrode in the absence and presence of the studied inhibitor was attained after 60–70 min from the moment of immersion. Corrosion current density (I_{corr}) of the investigated electrodes was determined [25], by extrapolation of cathodic and anodic Tafel lines to corrosion potential (E_{corr}). The inhibition efficiency expressed as percent inhibition ($\eta\%$) is defined as:

$$\eta\% = \frac{I_{uninh.} - I_{inh.}}{I_{uninh.}} \times 100 \quad (1)$$

where $I_{uninh.}$ and $I_{inh.}$ are the uninhibited and inhibited corrosion currents. The inhibited corrosion currents are those determined in the presence of the studied surfactants used in this investigation. The uninhibited corrosion currents were determined in pure (inhibitor free) CO_2-saturated 1% NaCl solution at the same temperature.

3. Results and discussion

3.1. Chemical structure of the synthesized surfactants

3.1.1. FT-IR spectroscopy

The structural characteristics of purified products of the synthesized acids (fatty acid and sulfated fatty acid) were confirmed by FT-IR spectroscopy in the range 4000–500 cm^{-1}, as shown in Fig. 1. These peaks of fatty acid are in accordance

Table 5 Test parameters for corrosion experiments, surface characterization and inhibitor characterization.

Material	Mild steel C1018
RCE outer surface area (cm^2)	4.55
Solution volume (L)	1.0
Temperature (°C)	20, 30, 40 and 50
pH	6.76 → 5.60
Inhibitor concentration (ppm)	10, 25, 50, 75 and 100
pCO_2 (bar)	0.90
NaCl concentration (wt%)	1.0
CO_2 quality	>99.7%
Solution stirring	Stirred
Scan rate (mV/s)	1.0
Inhibitors characterization	FT-IR
	Physical–chemical methods.
	Thermal analyses
Corrosion measurements	Extrapolation of cathodic and anodic Tafel plots
	Linear polarization corrosion rate
	Wight Loss measurements
Surface characterization	EDRF
	SEM

with the characteristic peaks of fatty acid reported in the literatures [26]. The peak at about 1709 cm^{-1} is due to the C═O carbonyl group of the carboxylic group, whereas the peak at 1550 cm^{-1} arises due to C═C bond. This bond was broken after the sulfating process. The peak at 1377 cm^{-1} is due to S–O stretching absorption bands. It indicates the almost complete removal of the C═C bond by the addition process.

3.1.2. Physical–chemical methods

Physical and chemical properties of fatty acid and sulfated fatty acid synthesized based on corn oil were studied and listed in Table 3. The data showed that, the acid number increased from 147.5 to 284 and no reaction with iodine after the sulfating process. These results confirmed, the complete removal of the C═C bond by the sulfating process and the formation of sulfated fatty acid.

From Table 4, it has been shown that, the freezing point of the synthesized inhibitors ranged between −24 and −19 °C, so that, these inhibitors can be used in countries with low temperatures.

3.1.3. Thermal analyses

Fig. 2 shows the TGA curves for the sodium salt of sulfated fatty acid (inhibitor I), results show that the evolution of composite material occurred through a three step process, It is seen that the first step for the total water loss was equal to 5.4% and 1st derivative of TG (DTG) revealed that the maximum water loss found at 140 °C can be linked to the loss of water of crystallization which is accompanied with a small endothermic in the DSC curve. In the second and third steps, the residual masses were 69%, 66% at 320, 528 °C, respectively and this is probably due to the decomposition of carboxylic acid (–C(═O)O) and the alkyl chain which is in a good agreement with the DSC peaks at 445, 545 °C. In the final step the residual mass was 61.19% at 578.9 °C which is related to the sulfated group (–O–SO_3). No sharp peaks of the DSC curves were seen up to 600 °C, showed that this salt did not undergo a significant change after this temperature.

3.2. Weight loss measurements

Fig. 3 shows the variation of the weight loss (in mg cm^{-2} d^{-1}) of mild steel with the immersion time in CO_2-saturated brine in the absence and presence of various concentrations (10–100 ppm) of inhibitor **V** (as example) at 50 °C. It is obvious from Fig. 3 that, the weight loss decreased, and therefore the corrosion inhibition strengthened, with increase in inhibitor concentration. This trend may result from the fact that adsorption and surface coverage increases with the increase in concentration; thus the surface is effectively separated from the medium [27].

As a result the surface coverage (θ) of compounds is increasing more clearly. This surface coverage (θ) is calculated using the following equation:

$$\theta = \frac{W_0 - W}{W_0} \tag{2}$$

where W_0 and W are the weight losses per unit area in the absence and presence of the inhibitor, respectively. The percentage inhibition efficiency, (η%), of the surfactants is calculated by applying the following equation [28,29].

$$\eta\% = \frac{W_0 - W}{W_0} \times 100 \tag{3}$$

The effect of the inhibitor concentration on the corrosion rate was examined; detailed experimental results were graphically represented in Fig. 4. At a given temperature (50 °C), a general trend is observed in the presence of the investigated inhibitors, a decrease in the weight loss of mild steel in the presence of these additives even at low concentration (10 ppm) compared to the blank (inhibitor free solution). By increasing the concentration of the surfactants, a further decrease in weight loss of mild steel was observed. The maximum inhibition efficiency (η%) for studied surfactants was obtained at 100 ppm, reach values close to their critical micellar concentration (CMC).

The results also indicate, that the percentage inhibition efficiency (η%) of the inhibitor (**V**) is greater than that of the

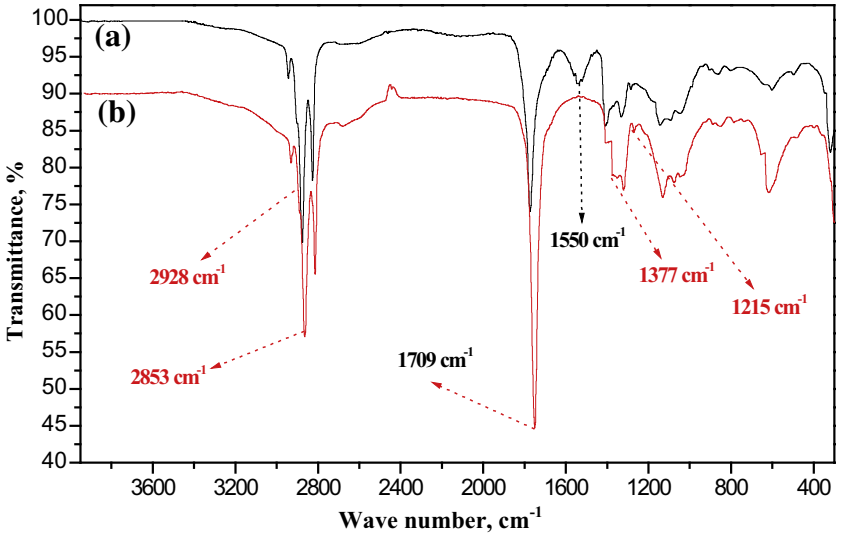

Figure 1 FTIR spectrum of (a) fatty acids derived from corn oil, (b) fatty acid after sulfating process.

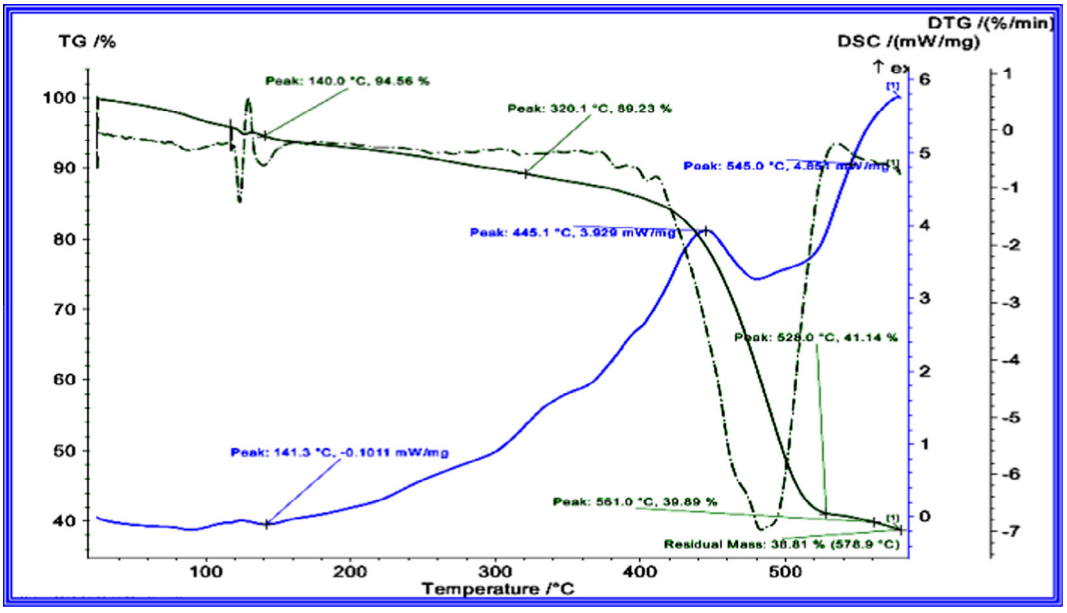

Figure 2 TG, DTG and DSC curves of the sodium salt of sulfated fatty acid (inhibitor **I**) in a flow of N_2 gas.

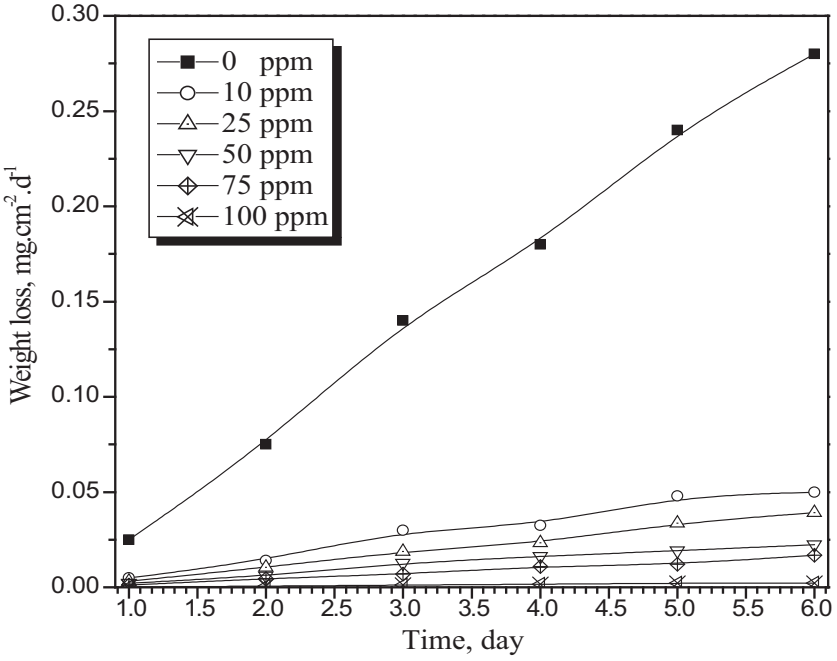

Figure 3 Weight loss–time curves of mild steel in CO_2–saturated brine in the absence and presence of different concentrations of inhibitor (**V**) at 50 °C.

other inhibitors. The inhibition efficiency of the surfactants decreases in the following order: **V** > **IV** > **III** > **I** > **II**. The highest inhibition efficiency of inhibitor **V** may be attributed to the following reasons:

I. The higher electron density on the functional groups leads to easier bond formation, greater adsorption, and consequently, higher inhibition.

II. The increase of the hydrocarbon chain length in the surfactant molecule means a more bulky molecule, which screens the surface from attack [30].

3.3. LPR corrosion rate

Figs. 5 and 6 show that, the change in corrosion rate (CR) with time for mild steel in CO_2-saturated 1% NaCl solution

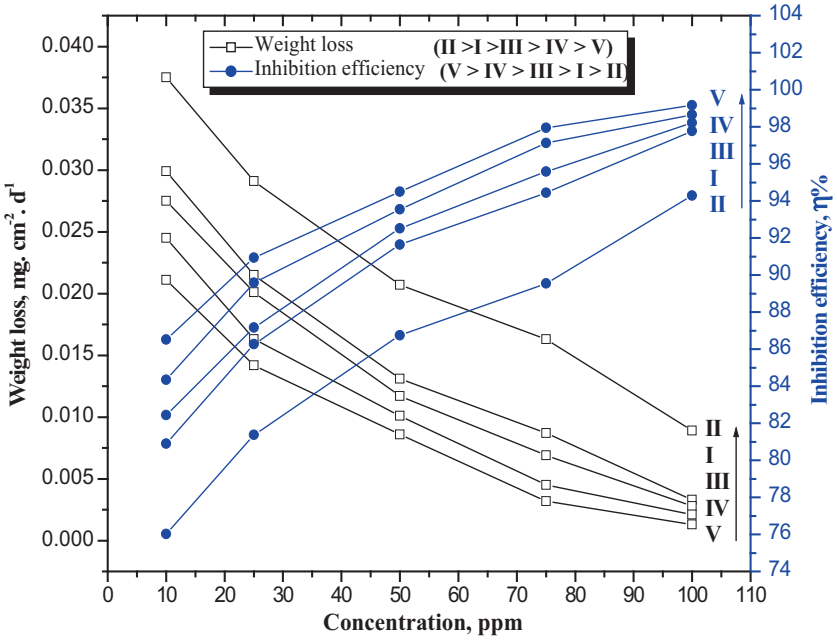

Figure 4 Weight loss and inhibition efficiency of mild steel immersed in CO_2 saturated brine with and without different inhibitors at 50 °C. (. . .) Weight loss, (–) inhibition efficiency.

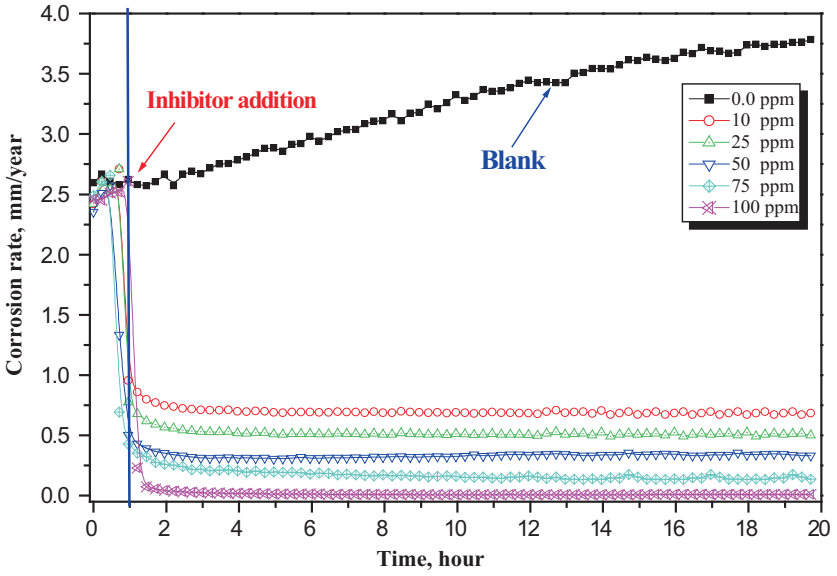

Figure 5 Variation of the corrosion rate with time for mild steel in CO_2-saturated brine containing different concentrations of inhibitor (**I**) at 50 °C.

containing different concentrations form inhibitors **I** and **V** at 50 °C (as examples). The inhibitor was added after 1 h of exposure because at this time the corrosion potential got stable, allowing the measurement of the CR prior the injection of the inhibitor. The initial corrosion rate, without inhibitor, was measured to be between 2.59 and 3.784 mm/year. It can be observed from Figs. 5 and 6 that the CR, in the absence of inhibitor, tends to increase with time. The increase in CR has been attributed to the galvanic effect between the ferrite phase and cementite (Fe_3C) which is a part of the original steel in the non-oxidized state and accumulates on the surface after the preferential dissolution of ferrite (α-Fe) into Fe^{2+} [31]. Fe_3C is known to be less active than the ferrite phase. Therefore, there is a preferential dissolution of ferrite over cementite, working the former as the anode and the latter as the cathode, favoring the hydrogen evolved reaction (HER) during the corrosion process [32,33].

Variation of the corrosion rate for inhibitors **I** and **V** at different concentrations is presented in Figs. 5 and 6. Corrosion parameters were calculated on the basis of LPR corrosion rate

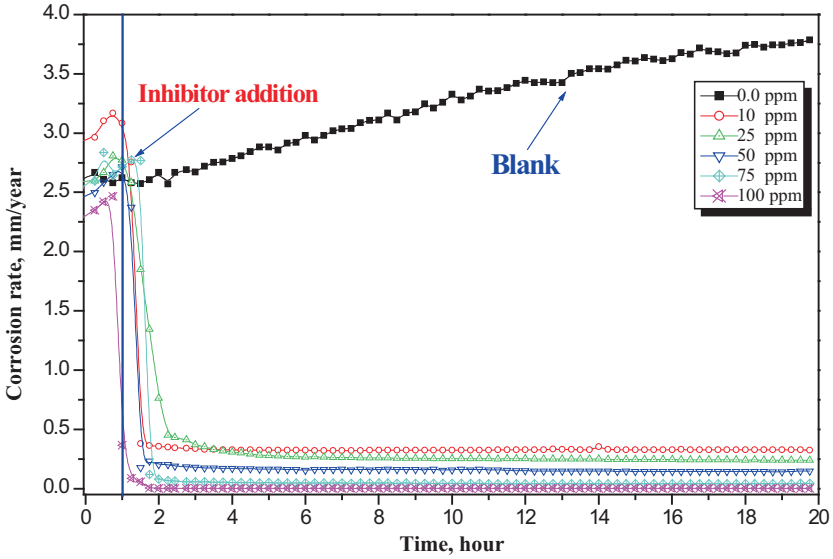

Figure 6 Variation of the corrosion rate with time for mild steel in CO_2-saturated brine containing different concentrations of inhibitor (**V**) at 50 °C.

test. The inhibition efficiency ($\eta\%$) and surface coverage (θ) were calculated according to the following equations:

$$\eta\% = \frac{CR_0 - CR_i}{CR_0} \times 100 \quad (4)$$

$$Surfacecoverage(\theta) = \theta = 1 - \frac{CR_i}{CR_0} \quad (5)$$

where CR_0 is the corrosion rate without inhibitor and CR_i is the corrosion rate when the inhibitor is present. It can be seen that the presence of inhibitors results a high decrease in the rate of corrosion. In the case of these inhibitors, the corrosion rate decreases as the inhibitor concentration increases, getting maximum inhibition efficiency that ranged between 98.55% and 99.95% at 100 ppm after 20 h of exposure (Table 6). This trend may result from the fact that adsorption and surface coverage increase with the increase in concentration; thus the surface is effectively separated from the medium [34].

Table 6 shows the calculated values of corrosion rates, the inhibition efficiencies and the surface coverage in the absence and presence of different concentrations of different inhibitors at 50 °C. The data exhibited that, the corrosion rates, the inhibition efficiencies and the surface coverage are found to depend on the concentrations of the inhibitors. The corrosion rate (CR) is decreased, and the inhibition efficiencies ($\eta\%$) and the surface coverage (θ) are increased with the increase of the surfactant concentrations. This indicates that the inhibitory action of the inhibitors against mild steel corrosion can be attributed to the adsorption of these molecules on the metal surface, limits the dissolution of mild steel, and the adsorption amounts of surfactants on mild steel increase with concentrations in the corrosive solutions.

Fig. 7 shows the variation of the corrosion rate with time for mild steel in CO_2-saturated 1% NaCl solution containing 100 ppm from different surfactants at 50 °C. This plot indicates that, the presence of different inhibitors decreases the rate of corrosion. However, the maximum decrease in the corrosion rate was observed for inhibitor (**V**) and the inhibition efficiency of the investigated inhibitors was increased in the following order: **V** > **IV** > **III** > **I** > **II** (after 20 h). This could be attributed to the increase of the electron densities and the molecular size [35].

3.4. Extrapolation of cathodic and anodic Tafel lines

Fig. 8 shows the influence of inhibitor **V** concentrations on the Tafel cathodic and anodic polarization characteristics of mild steel in CO2-saturated solution at a scan rate of 1 mV/s and at 50 °C. Corrosion parameters were calculated on the basis of cathodic and anodic potential versus current density characteristics in the Tafel potential region [36,37]. The values of the corrosion current density (I_{corr}) for the investigated metal without and with the inhibitor were determined by the extrapolation of cathodic and anodic Tafel lines to the corrosion potential (E_{corr}). It can be seen that the presence of surfactant molecules results in a marked shift in both cathodic and anodic branches of the polarization curves toward lower current densities. This means that, the inhibitors affect both cathodic and anodic reactions. It was found that, both anodic and cathodic reactions of mild steel electrode corrosion were inhibited with increasing concentration of the synthesized inhibitors. These results suggest that not only the addition of synthesized inhibitors reduce anodic dissolution but also retard the hydrogen evolution reaction. The results showed that the inhibiting action of these inhibitors on both cathodic and anodic processes seems to approximately be equal. The inhibitor may decrease the corrosion through the reduction of mild steel reactivity. According to this mechanism, a reduction of either the anodic or the cathodic reaction or both arises from the adsorption of the inhibitor on the corresponding active sites [38].

The electrochemical parameters E_{corr}, I_{corr}, inhibition efficiency ($\eta\%$), anodic and cathodic Tafel slopes (β_a, β_c) obtained from the polarization measurements were listed in Table 7. The data exhibited that, the corrosion current density (I_{corr}) decreases, and the inhibition efficiency ($\eta\%$) increases as the concentration of inhibitors is increased. These results suggest

Table 6 The corrosion parameters for mild steel electrode in CO_2-saturated solution in the absence and presence of various concentrations of inhibitors at 50 °C.

Inhibitors code	Surfactant concentration (ppm)	Corrosion rate (mm/year)	Surface coverage (θ)	The inhibition efficiency, (η%)
CO_2-saturated 1% NaCl solution without inhibitor	0.0	3.784	–	–
I	10	0.685	0.81	81.1
	25	0.501	0.86	86.7
	50	0.332	0.91	91.2
	75	0.135	0.96	96.4
	100	0.010	0.99	99.7
II	10	0.715	0.81	81.0
	25	0.559	0.85	85.2
	50	0.404	0.89	89.3
	75	0.161	0.95	95.7
	100	0.054	0.98	98.5
III	10	0.583	0.84	84.5
	25	0.449	0.88	88.1
	50	0.223	0.94	94.0
	75	0.117	0.96	96.8
	100	0.004	0.99	99.8
IV	10	0.374	0.90	90.0
	25	0.279	0.92	92.6
	50	0.179	0.95	95.2
	57	0.068	0.98	98.1
	100	0.002	0.99	99.9
V	10	0.324	0.91	91.4
	25	0.238	0.93	93.6
	50	0.146	0.96	96.1
	75	0.043	0.98	98.8
	100	0.001	0.99	99.9

that retardation of the electrodes processes occurs, at both cathodic and anodic sites, as a result of coverage of these sites by surfactant molecules. However, the maximum decrease in I_{corr} was observed for (**V**). This could be attributed to the increase of the electron densities and the molecular size [35,39]. The increase of inhibitor efficiency with increasing of the concentration can be interpreted on the basis of the adsorption amount and the coverage of surfactant molecules, increases with increasing concentrations [40]. The E_{corr} values of all synthesized inhibitors were shifted slightly toward both cathodic and anodic directions and did not show any definite trend in CO2-saturated brine. This may be considered due to the mixed-type behavior of the studied inhibitors. The shift in E_{corr} that is characteristic of anodic and anodic/cathodic inhibitors is observed[41]. It was explained that this shift in E_{corr} is due to an active site blocking effect that occurs when an inhibitor is added [42]. In the case of CO_2 corrosion the anodic and cathodic reactions are due the oxidation of iron and the reduction of hydrogen, respectively [43]. If it is considered that the active sites on the metal surface are the same for both reactions before adding the inhibitor, it is logical that the change in E_{corr} occurs when the inhibitor is present because its adsorption changes those active sites and therefore the anodic and cathodic reaction rates [44].

The fact is that the slopes of the cathodic (β_c) and anodic (β_a) Tafel lines in Table 7 are approximately constant and independent of inhibitor concentration. These results indicate that these inhibitors act by simply blocking the available surface area. In other words, the inhibitor decreases the surface area for corrosion of the investigated metal, and only causes inactivation of a part of the surface with respect to the corrosive medium [40]. On the other hand, the anodic Tafel slopes (β_a) are also found to be greater than the respective cathodic Tafel slopes (β_c). These observations are correlated with the fact that the anodic exchange-current density values are less than those of the cathodic counter parts. It can be concluded that the overall kinetics of corrosion of the mild steel alloy in CO_2 saturated solution is under anodic control.

Data in Table 7 show that the inhibition efficiency increased with increasing the inhibitor concentrations. The inhibition efficiency of the investigated inhibitors was increased in the following order: **V** > **IV** > **III** > **I** > **II**. The inhibition efficiencies are in a good agreement with those calculated from the weight loss measurements and the LPR corrosion rate.

The high inhibition efficiency obtained in CO_2-saturated solution in the presence of studied inhibitors by all investigated methods can be attributed to the formation of a protective film of iron carbonate ($FeCO_3$) as follows [45]:

$$CO_{2(g)} \leftrightarrow CO_{2(aq)} \tag{6}$$

$$CO_{2(aq)} + H_2O \leftrightarrow H_2CO_{3(aq)} \tag{7}$$

$$H_2CO_{3(aq)} \leftrightarrow H^+ + HCO_3^- \tag{8}$$

$$HCO_3^- \leftrightarrow H^+ + CO_3^{2-} \tag{9}$$

The anodic dissolution for iron in carbonic acid solutions gives ferrous ions [45].

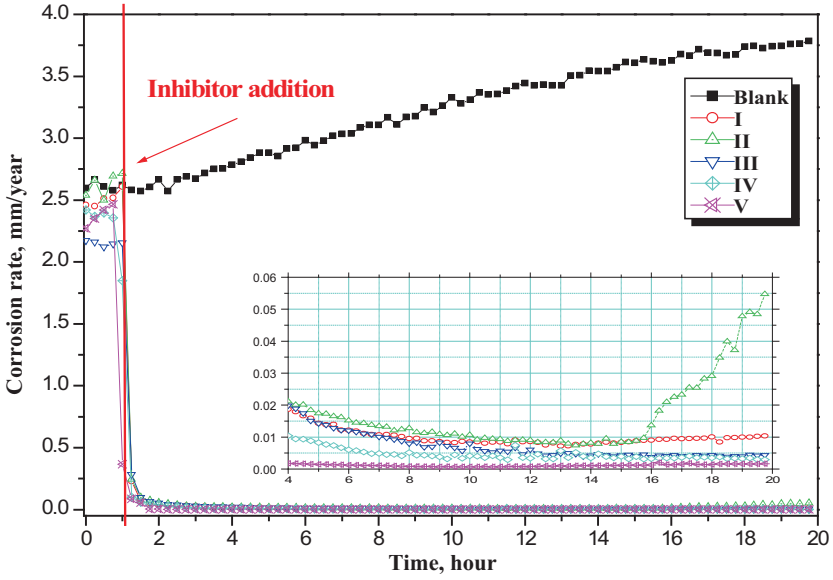

Figure 7 Variation of the corrosion rate with time for mild steel in CO_2-saturated brine containing 100 ppm from different inhibitors at 50 °C.

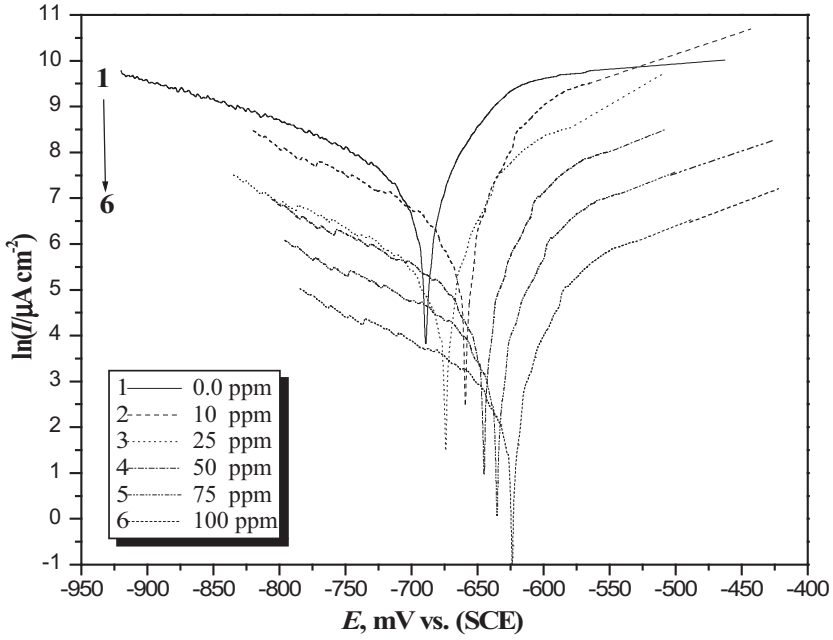

Figure 8 Cathodic and anodic Tafel polarization curves for mild steel in CO_2-saturated brine containing different concentrations of inhibitor **V** at 50 °C.

$$Fe \leftrightarrow Fe^{2+} + 2e^{-} \quad (10)$$

According to these processes, a corrosion layer was formed on the steel surface. The properties of the formed layers and its effect on the corrosion rate are important factors to take into account when studying the corrosion of steel in CO_2 environments. Ogundele and White suggested that, iron carbonate, $FeCO_3$, may be important in the formation of protective layers on the steel surface [46]. The formation of iron carbonate can be explained by using the following equation [47].

$$Fe^{2+} + CO_3^{2-} \rightarrow FeCO_3 \quad (11)$$

3.5. Surface tension and surface active properties

The main importance of the critical micelle concentration (CMC) consists of the fact that at this concentration, most of the physical and chemical properties of the surfactant solutions present an abrupt variation. The values of surface tension (γ) were measured at 298 K for various concentrations of the

Table 7 Corrosion parameters obtained from Tafel polarization for mild steel in CO_2-saturted solution in the absence and presence of different concentrations of the prepared surfactants at 50 °C.

Inhibitors code	Conc. of inhibitor (ppm)	E_{corr} (mV(SCE))	I_{corr} (μA cm^{-2})	β_a (mV dec^{-1})	$-\beta_c$ (mV dec^{-1})	θ	η%
Absence	0.0	−689	2100	175	124	–	–
I	10	−665	412	172	120	0.80	80.3
	25	−681	296	169	121	0.85	85.8
	50	−651	203	175	121	0.90	90.2
	75	−649	95	173	123	0.95	95.4
	100	−641	26	165	122	0.98	98.7
II	10	−661	414	175	117	0.80	80.2
	25	−655	328	176	121	0.84	84.3
	50	−660	243	185	118	0.88	88.4
	75	−649	109	180	120	0.94	94.7
	100	−637	51	181	119	0.97	97.5
III	10	−662	341	165	121	0.83	83.7
	25	−651	267	172	125	0.87	87.2
	50	−654	144	166	122	0.93	93.1
	75	−647	85	171	124	0.95	95.9
	100	−634	23	169	123	0.98	98.8
IV	10	−665	227	177	124	0.89	89.1
	25	−653	174	180	128	0.91	91.6
	50	−661	119	178	125	0.94	94.2
	75	−641	58	177	127	0.97	97.2
	100	−632	22	171	126	0.98	98.9
V	10	−660	199	173	125	0.90	90.5
	25	−673	152	185	130	0.92	92.7
	50	−643	101	180	127	0.95	95.1
	75	−635	44	172	128	0.97	97.8
	100	−623	21	179	126	0.98	98.9

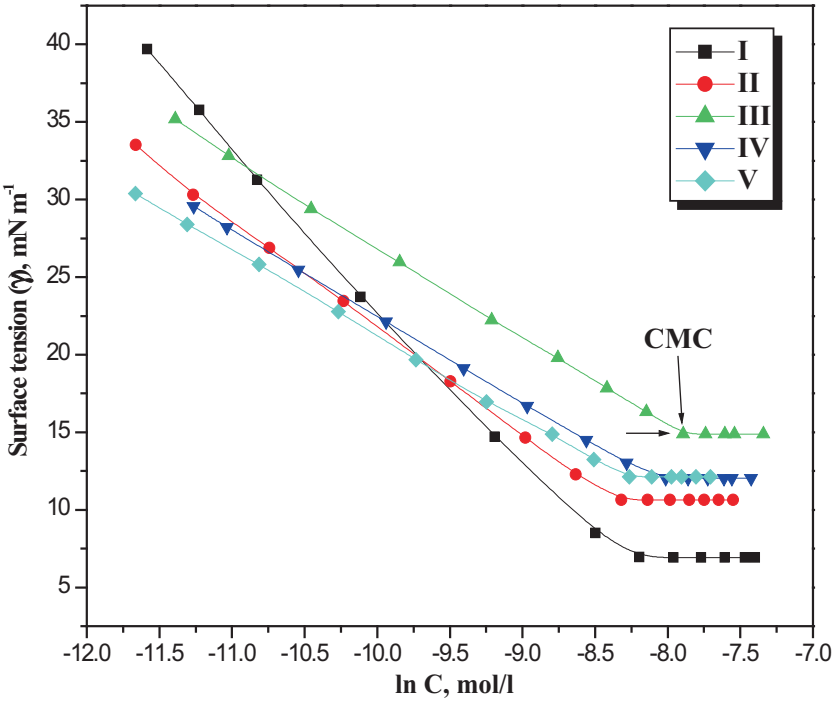

Figure 9 Change of surface tension (γ) with the concentration of the surfactants at 298 K.

surfactants. The measured values of (γ) were plotted against the surfactant concentration, ln C (Fig. 9). This figure showed two characteristic regions. The first at low concentrations and characterized by continuous decrease of the surface tension values due to the adsorption of surfactant molecules at the interface. The second region locates at higher surfactant concentrations where the surface tension values are almost stable [48,49]. The intercept of the two straight lines designates the critical micelle concentration (CMC), where saturation in the surface adsorbed layer takes place. The surface active properties of the surfactants; effectiveness (π_{cmc}), maximum surface excess (Γ_{max}) and minimum area per molecule (A_{min}) were calculated using the following equations [50]:

$$\pi_{cmc} = \gamma_0 - \gamma_{cmc} \tag{12}$$

$$\Gamma_{max} = \frac{-1}{RT[\partial\gamma/\partial \ln C]_T} \tag{13}$$

$$A_{min} = \frac{1}{\Gamma_{max} \times N_A} \tag{14}$$

where $\partial\gamma/\partial \ln C$ is the maximum slope, γ_0 is the surface tension of pure water, γ_{cmc} is the surface tension at critical micelle concentration, N_A is the Avogadro's number (6.023×10^{23} molecules/mol), R is the molar gas constant (R = 8.314 J/mol K) and T is the absolute temperature.

The standard free energy of micellization and adsorption is given by [51]:

$$\Delta G^{\circ}_{mic} = RT \ln \mathrm{CMC} \tag{15}$$

$$\Delta G^{\circ}_{ads} = \Delta G^{\circ}_{mic} - 0.6023\pi_{CMC}A_{min} \tag{16}$$

The data obtained from surface tension measurements were summarized and presented in Table 8. The values of effectiveness (π_{cmc}) at 298 K indicate that the prepared compounds give large reduction of surface tension at CMC, so that, these compounds act as effective corrosion inhibitors for mild steel in CO_2-saturated brine.

From Table 8 it can be seen that the values of ΔG°_{mic} and ΔG°_{ads} are always negative, indicating the spontaneity of these two processes, but there is more increase in negativity of ΔG°_{ads} than of ΔG°_{mic}, indicating the tendency of the molecules to be adsorbed at the interface [51].

3.6. Effect of surfactant concentration on corrosion inhibition

The data obtained from all the used methods are in a good agreement with each other. The inhibition efficiency increased as the surfactant concentrations are increased as shown in Tables 6 and 7. It was obvious that, the inhibition efficiency for inhibitor **V** (as an example) at 10 ppm was 91.4%; at 50 ppm was 96.12% and at 100 ppm was 99.95% indicating that, there was an ascending order in the inhibition efficiency with increasing concentration for all the surfactant inhibitors. Consequently, the corrosion rate was concentration dependent. In more detail, in low concentrations, the surfactant monomers were adsorbed as individual ions/molecules without mutual interactions. At higher concentrations, tail–tail interactions of surfactants may begin to cause an association of aggregates adsorbed into an additional coverage beyond the monolayer, i.e. admicelles or bilayer formation. The surfactant monomers head groups of the first layer face the surface while those of the second layer face the bulk solution. Thus the increase in concentration of surfactant solutions increases the surface coverage from coverage at lower surfactant to bilayer coverage at higher surfactant concentrations. Fig. 10 shows a schematic representation of the inhibitor adsorption on mild steel surface (10a), adsorption as single molecule at low concentration (10b), hemimicelle formation at higher concentration (10c), and formation of multi-layers at very high concentrations [19,52].

Table 8 The critical micelle concentration and surface parameters of the synthesized surfactants.

Inhibitors code	CMC (mM)	γ_{cmc} (mN m^{-1})	π_{cmc} (mN m^{-1})	Γ_{max} (mol cm^{-2})×10^{-10}	A_{min} (nm^2)	ΔG°_{mic} (kJ/mol)	ΔG°_{ads} (kJ/mol)
I	0.27	6.98	65.02	5.01	0.331	−20.3	−33.2
II	0.24	10.61	61.39	6.99	0.234	−20.6	−29.3
III	0.37	15.06	56.94	7.63	0.217	−19.5	−27.0
IV	0.33	12.52	59.48	8.39	0.197	−19.8	−26.8
V	0.25	11.92	60.08	8.33	0.199	−20.4	−27.7

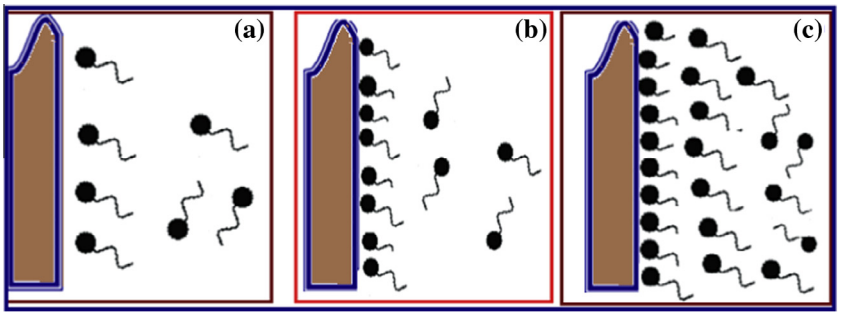

Figure 10 Schematic representation of the inhibitor adsorption on mild steel surface. (a) Adsorption as single molecule at low concentration. (b) Hemimicelle formation at higher concentration. (c) Formation of multi-layers at very high concentration.

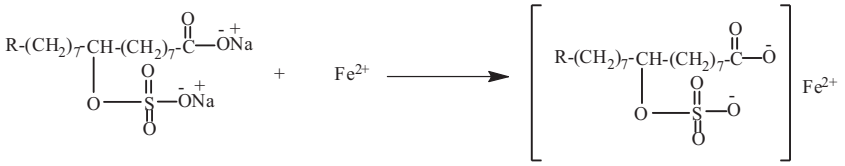

Figure 11 Ionic form suggested to be formed on the mild steel surface.

The adsorption of synthesized surfactants on the metal surface can occur either directly on the basis of donor–acceptor interactions between the oxygen or sulfur groups and the vacant d-orbitals of steel surface atoms (inhibitors **I**, **II** and **III**) or an interaction of organic nitrogen compounds (inhibitors **IV** and **V**) with already adsorbed groups. Immediately afterward, as the corrosion reaction starts, ferrous ion is surrounded by two oxygen atoms at Fe–O(COO^-) and Fe–O(OSO_3^-) as explained in Fig. 11. These results were confirmed by FT-IR. The data for inhibitor **I** (SSFA) showed that, S═O stretching frequency drops from the level of 1350 cm^{-1} to the level of 1320 cm^{-1}. This suggests that the electron cloud of S═O is shifted from S═O up to Fe^{2+} resulting in the formation of Fe^{2+}–SSFA complex on the metal surface.

There was an increase in the efficiency of corrosion inhibition with increasing concentration, since the adsorption of C═O, oxygen, nitrogen and sulfur groups onto the metal surface was stronger, and effectively protecting the surface. Conclusively, the surfactant inhibitor, having near unity θ (see Tables 6 and 7), was considered as a good physical barrier shielding the corroding surface from corrosive medium and dumping the corrosion rate of mild steel significantly.

3.7. Adsorption isotherm and thermodynamic parameters for the corrosion process

Classical adsorption isotherms have been used extensively in the study of adsorption of organic substances onto steel electrodes. It is widely acknowledged that they provide useful insights into the mechanism of corrosion inhibition [53]. A determination of the type of adsorption isotherm itself provides information on the adsorption process such as surface coverage, adsorption equilibrium constant and information on the interaction between the organic compound and electrode surface [24].

The interaction between the inhibitors and mild steel surface can be described by the adsorption isotherm. During corrosion inhibition of metals, the nature of the inhibitor on the corroding surface has been deduced in terms of adsorption characteristics of the inhibitor. Furthermore, the solvent (H_2O) molecules could also be adsorbed at metal/solution interface. So the adsorption of surfactants molecules from aqueous solution can be regarded as a quasi-substitution process between the organic compounds in the aqueous phase [$Surfactant_{(sol.)}$] and water molecules at the electrode surface [$H_2O_{(ads)}$] [54]:

$$Surfactant_{(sol.)} + mH_2O_{(ads.)} = Surfactant_{(ads.)} + mH_2O_{(sol.)} \quad (17)$$

where m is the size ratio, that is, the number of water molecules replaced by one organic inhibitor. Basic information on the interaction between the inhibitor and the mild steel surface can be provided by the adsorption isotherm. In order to obtain the isotherm, the linear relation between the degree of surface coverage (θ) and inhibitor concentration (C) must be found. Attempts were made to fit the θ values to various isotherms including Langmuir, Temkin, Frumkin and Flory–Huggins. By far the best fit was obtained with the Langmuir isotherm. The Langmuir isotherm is based on the assumption that all adsorption sites are equivalent and that particle binding occurs independently from nearby sites, whether occupied or not [55]. According to this isotherm, θ is related to C by:

$$\frac{C_{inh}}{\theta} = C_{inh} + \frac{1}{K_{ads}} \quad (18)$$

where K_{ads} is the equilibrium constant of the inhibitor adsorption process and C_{inh} is the surfactant concentration.

Fig. 12 shows the plots of C/θ against inhibitor concentrations (C) at 323 K and the expected linear relationship is obtained for all surfactants with excellent correlation coefficients (R^2) (Table 9), confirming the validity of this approach. The slopes of the straight lines are unity, suggesting that adsorbed surfactant molecules form a monolayer on the mild steel surface and there is no interaction among the adsorbed inhibitor molecules.

The values of K_{ads} obtained from the Langmuir adsorption isotherm are listed in Table 9, together with the values of the Gibbs free energy of adsorption (ΔG°_{ads}) calculated from [54]:

$$K_{ads} = \frac{1}{55.5}\exp\left(-\frac{\Delta G^{\circ}_{ads}}{RT}\right) \quad (19)$$

where R is the universal gas constant, T is the thermodynamic temperature and the value of 55.5 is the concentration of water in the solution [56].

The high values of K_{ads} for studied surfactants indicate stronger adsorption on the mild steel surface in CO_2-saturated solution. It is also noted that, the high values of K_{ads} for surfactants **V** and **IV** indicate stronger adsorption on the mild steel surface than the surfactants **I**, **II** and **III**. This can be simply explained by the presence of additional donor atoms, such as nitrogen, in the appended functional groups. Large values of K_{ads} imply more efficient adsorption and hence better inhibition efficiency [57]. The large value of K_{ads} obtained for the studied surfactants agree with the high inhibition efficiency obtained.

Generally, values of ΔG°_{ads} up to -20 kJ mol^{-1} are consistent with physisorption, while those around -40 kJ mol^{-1} or higher are associated with chemisorption as a result of the sharing or transfer of electrons from organic molecules to the metal surface to form a coordinate bond [58,59]. In the present study, the values of ΔG°_{ads} obtained for the studied surfactants on mild steel in CO_2-saturated solution ranges between -42.54 and -44.12 kJ mol^{-1}, which are more than -40 kJ mol^{-1} (Table 9). These results indicate that the adsorption mechanism of surfactants on mild steel in CO_2 saturated

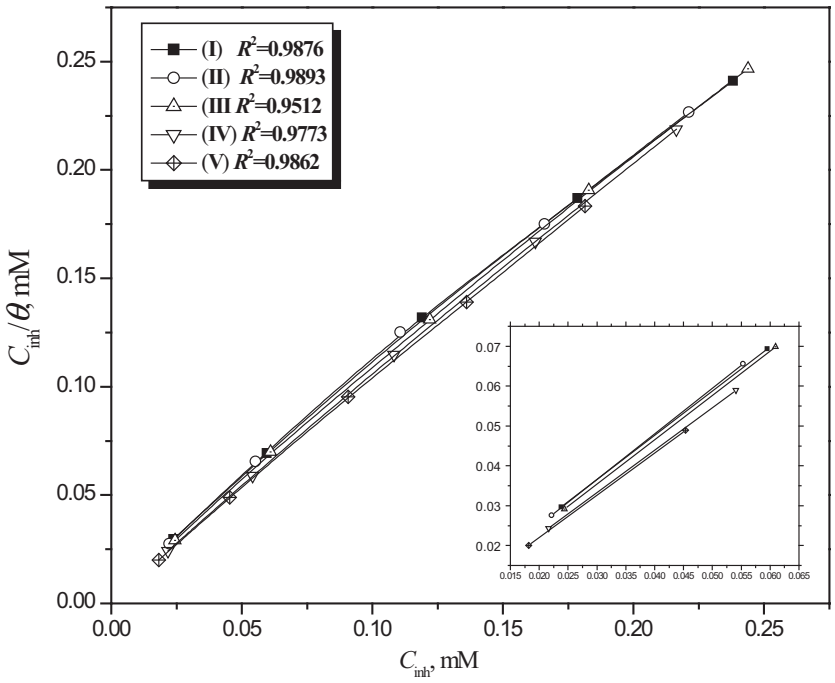

Figure 12 Langmuir adsorption isotherm (C_i/θ vs. C_i) from Tafel polarization data for mild steel in CO_2 saturated brine containing various concentrations of inhibitors at 50 °C.

Table 9 Thermodynamic parameters for the adsorption of the studied surfactants on mild steel electrode in CO_2-saturated solution.

Inhibitors code	Slope	Regression coefficients, R^2	K_{ads}, M^{-1}	ΔG°_{ads} (kJ mol^{-1})	$\Delta H^{\circ}_{ads.}$ (kJ/mol)	$\Delta S^{\circ}_{ads.}$ (J/mol K)
I	1.03	0.9876	8.65×10^4	−42.9	−42.6	11.0
II	1.08	0.9893	8.16×10^4	−42.5	−42.1	11.4
III	1.03	0.9512	8.79×10^4	−43.0	−42.6	10.7
IV	1.02	0.9773	11.82×10^4	−43.7	−43.3	10.6
V	1.01	0.9862	13.84×10^4	−44.1	−43.7	11.4

solution is typical of chemisorption at the studied temperatures. Chemisorption of the surfactant molecules could occur due to the formation of links between the d orbital of iron atoms, involving the displacement of water molecules from the metal surface, and the lone sp^2 electron pairs present on the N, S and/or O atoms of the inhibitor. The high and negative values obtained for ΔG°_{ads} indicate that the adsorption process takes place spontaneously by strong interactions between the inhibitor and the steel surface, as was suggested by the obtained values of $K_{ads.}$ Thermodynamically, ΔG°_{ads} is related to the enthalpy and entropy of adsorption process, $\Delta H^{\circ}_{ads.}$ and $\Delta S^{\circ}_{ads.}$, respectively, by the equation:

$$\Delta G^{\circ}_{ads.} = \Delta H^{\circ}_{ads.} - T\Delta S^{\circ}_{ads.} \quad (20)$$

Fig. 13 shows the plot of ΔG°_{ads} vs. T which gives a straight line with an intercept of $\Delta H^{\circ}_{ads.}$ and a slope of $-\Delta S^{\circ}_{ads.}$ [60]. Adsorption is generally accompanied by the release of energy, that is, most adsorption processes are exothermic in nature. An endothermic adsorption process ($\Delta H^{\circ}_{ads.} > 0$) signifies unequivocally chemisorption, while an exothermic adsorption process ($\Delta H^{\circ}_{ads.} < 0$) may involve either physisorption or chemisorption or a mixture of both the two processes [57,60]. The calculated values of $\Delta H^{\circ}_{ads.}$, $\Delta S^{\circ}_{ads.}$ for mild steel in CO_2-saturated solution containing various concentrations from surfactants are listed in Table 9. The negative value of $\Delta H^{\circ}_{ads.}$ indicates that, the adsorption of the inhibitor molecule is an exothermic process [61]. The magnitude of positive $\Delta S^{\circ}_{ads.}$ and negative $\Delta H^{\circ}_{ads.}$ values indicate the occurrence of a replacement process during adsorption of inhibitor molecules on the mild steel surface [62].

3.8. Effect of temperature on the corrosion inhibition

In order to gain more information about the type of adsorption and the effectiveness of the studied inhibitors at higher temperatures, cathodic and anodic Tafel polarizations were performed at different temperatures (20–50 °C) for mild steel in CO_2-saturated 1.0% NaCl solution without and with selected concentrations of the studied surfactants. The data in Fig. 14 exhibit that the inhibition efficiency for mild steel in the presence of inhibitors **I** and **V** (as example) increases with increasing temperature, indicate that the inhibitors are more effective at higher temperatures up to 50 °C. This behavior may be due to the increase in the strength of adsorption process at higher temperatures, suggesting that chemisorption may be the type of adsorption of the inhibitors molecules on mild steel surface. Thus, the predominance of corrosion

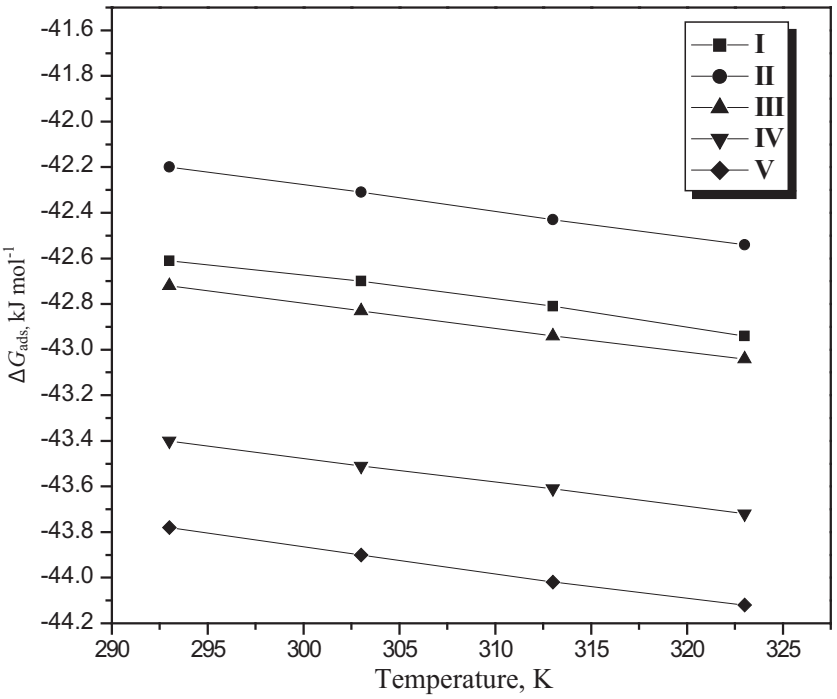

Figure 13 Variation of ΔG°_{ads} vs. T on mild steel in CO_2-saturated brine containing the surfactant inhibitors.

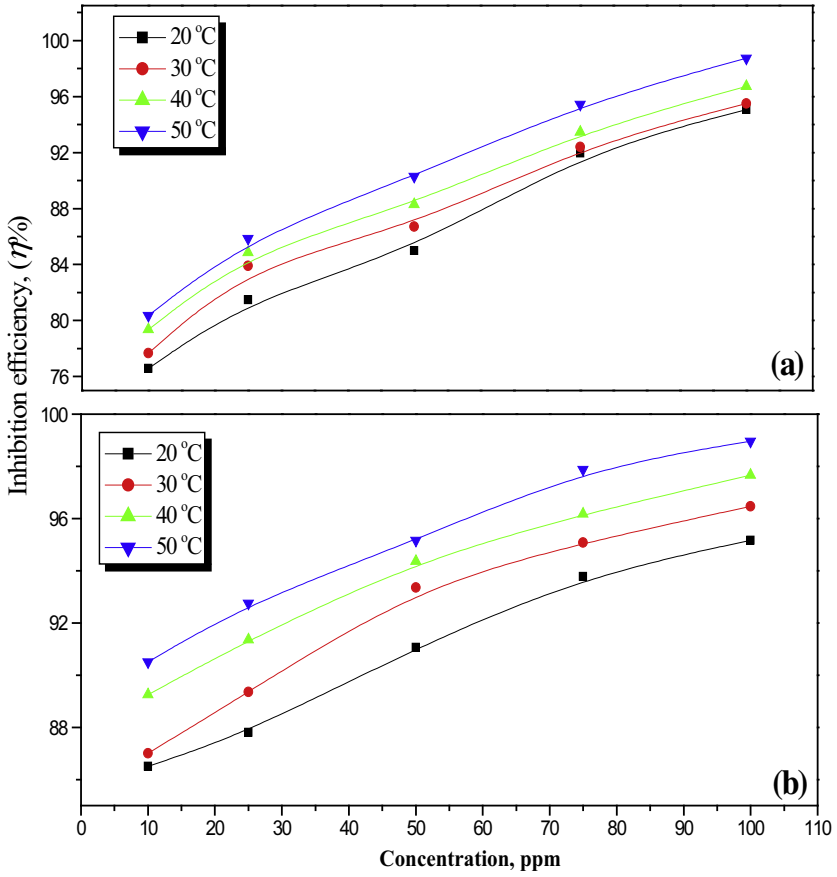

Figure 14 Effect of various concentrations of (a) inhibitor **I** (b) inhibitor **V** on the inhibition efficiency of mild steel in CO_2-saturated solution at different temperatures.

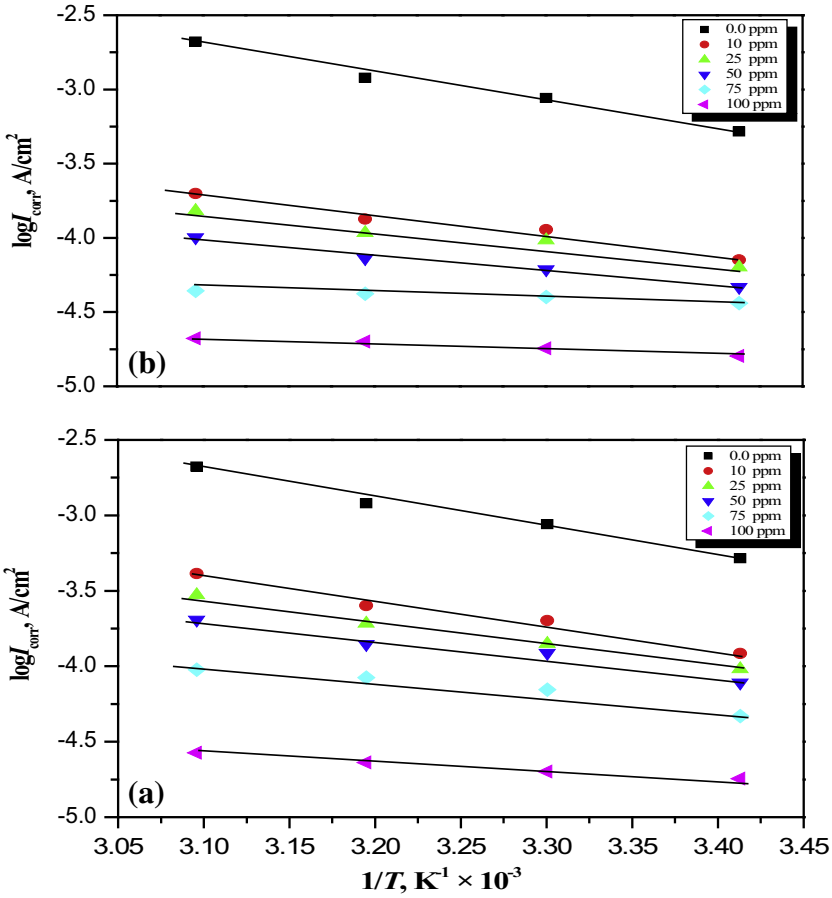

Figure 15 Arrhenius plots for mild steel corrosion in CO_2-saturated brine containing various concentrations of (a) inhibitor **I** and (b) inhibitor **V**.

inhibition for mild steel using studied surfactants, suggests an appreciable contribution to the inhibition process via the formation of Fe^{2+}-surfactants complex on the metal surface.

However, increasing the solution temperature (inhibited and blank solution) leads to an increase in the current density values. Moreover slight cathodic shifts are observed in E_{corr} values at higher temperatures (not mentioned in the text). This result reflects enhancement of the cathodic hydrogen evolution reaction with temperature. Similar results were obtained by Hassan [60] for corrosion inhibition of mild steel by triazole derivatives in HCl solution .The increase of corrosion rate is pronounced with a rise of temperature [63]. However, the values of η% increase with temperature until reaching their plateau value at about 99.8% for inhibitor **V** at 100 ppm and 50 °C.

Arrhenius plots for mild steel in the absence and presence of investigated inhibitor in 1% solution of NaCl saturated with CO_2 are shown in Fig. 15. The activation energy can be expressed by the Arrhenius equation:

$$\log I_{corr} = \log A - \frac{E_a}{2.33R}\frac{1}{T} \quad (21)$$

where I_{corr} is the corrosion current density obtained from Tafel plot, A is an Arrhenius pre-exponential factor, E_a is the apparent activation energy of the corrosion process, T is the absolute temperature and R is the universal gas constant [64]. Some relevant information about the adsorption mechanism of the

Table 10 Apparent activation energy in kJ/mol for mild steel in CO_2-saturated solution containing various concentrations of inhibitors **I** and **V**.

Inhibitors code	Concentration (ppm)	E_a (kJ/mol)
Without inhibitor	0.0	30.62
I		
	10	29.73
	25	29.31
	50	24.01
	75	18.53
	100	10.46
V		
	10	25.93
	25	21.85
	50	19.75
	75	7.36
	100	4.97

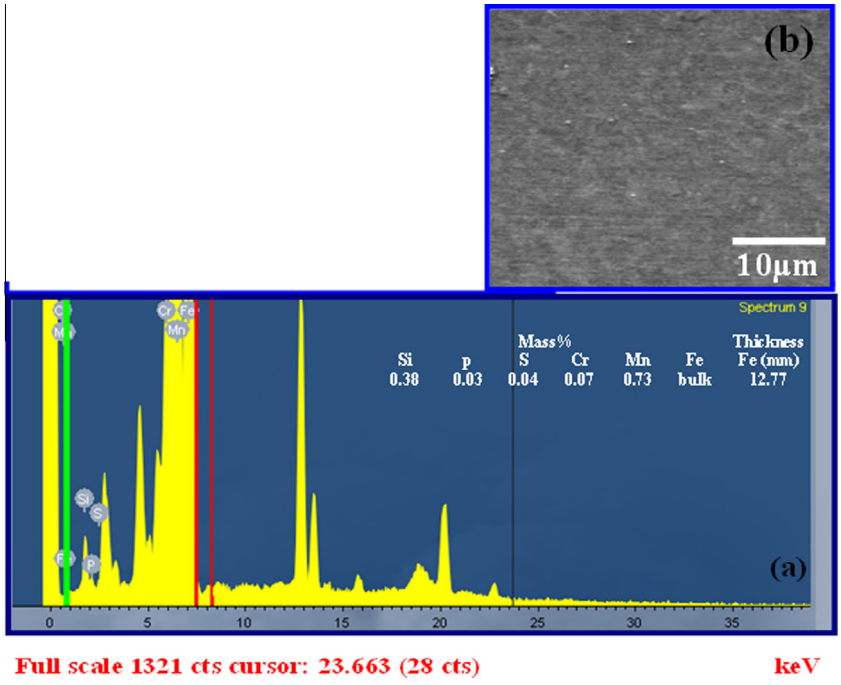

Figure 16 EDRF analysis of mild steel electrode surface (a) and SEM picture of mild steel electrode surface at magnification × = 1000 (b).

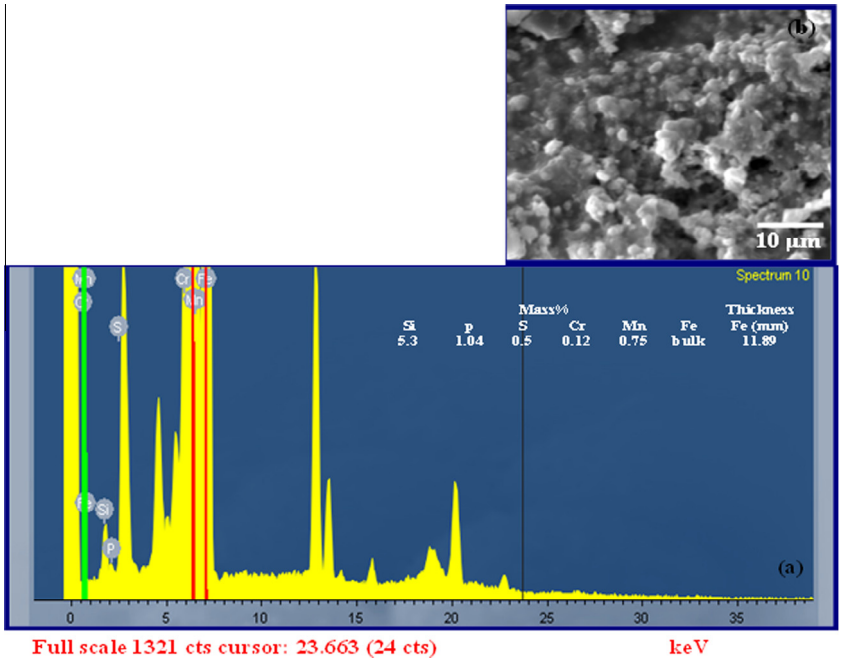

Figure 17 EDRF analysis of mild steel electrode surface after immersion in CO_2-saturated brine for 6 days without inhibitor (a) and SEM picture at the same conditions at magnification × = 1000 (b).

inhibitor can be obtained by comparing E_a both in the absence and presence of the corrosion inhibitor.

Values of the apparent activation energy of corrosion for mild steel in CO_2 saturated brine in the absence and presence of different concentrations of inhibitors **I** and **V** (as examples) were determined from the slope of log I_{corr} vs. $1/T$ plots and are given in Table 10. Activation energy value of the corrosion process in the absence of the inhibitor in 1.0% NaCl saturated solution is 30.62 kJ mol^{-1}, which is close to the value obtained by Okafor et al. (28.60 kJ mol^{-1}) [3].

The activation energy decreases as the concentration of inhibitors increases from 10 to 100 ppm. This can be explained as due to the enhancement of the inhibitor adsorption onto the metal surface at higher temperatures. Thus an increase in the

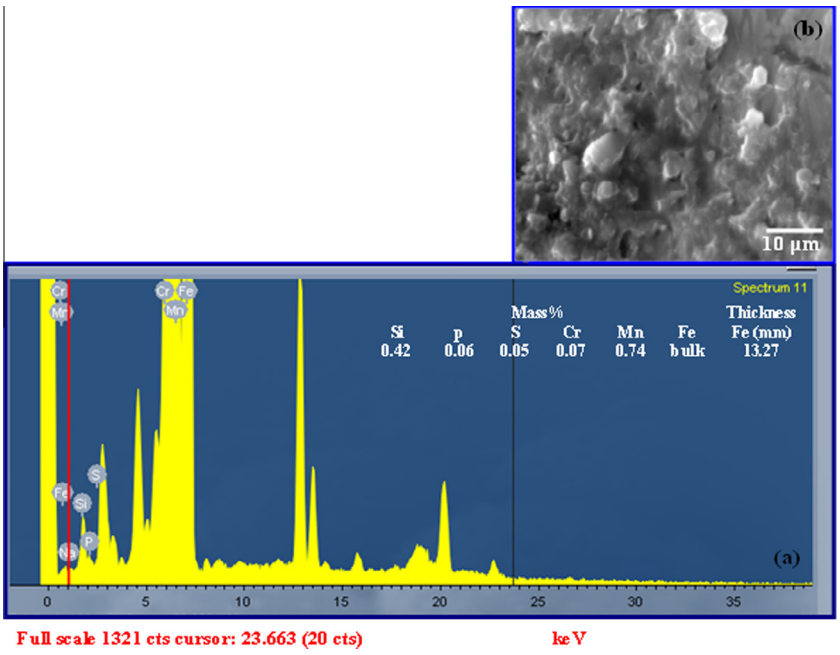

Figure 18 EDRF analysis of mild steel electrode surface after immersion in CO_2-saturated brine + 100 ppm inhibitor **I** for 6 days (a) and SEM picture at the same conditions at magnification × = 1000 (b).

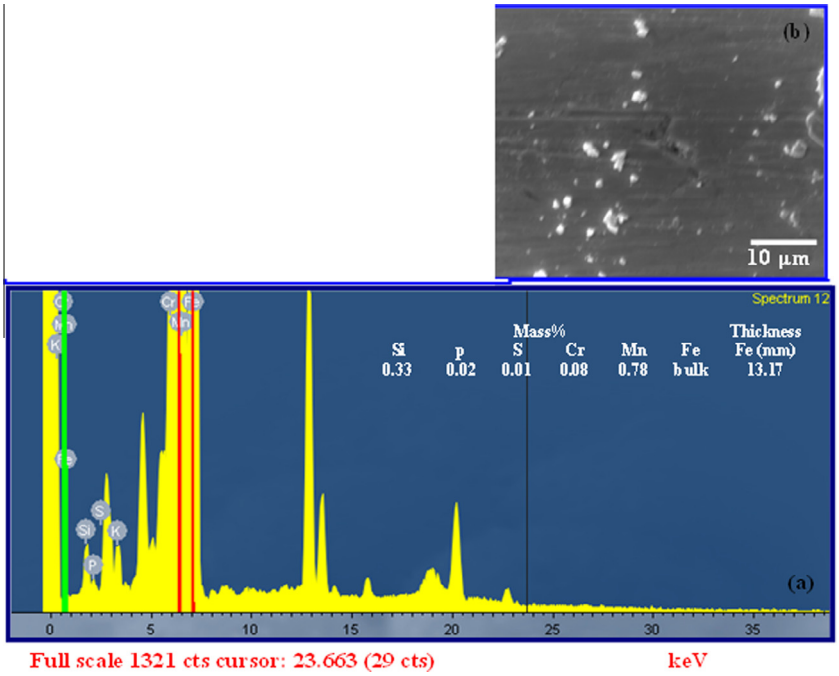

Figure 19 EDRF analysis of mild steel electrode surface after immersion in CO_2-saturated brine + 100 ppm inhibitor **II** for 6 days (a) and SEM picture at the same conditions at magnification × = 1000 (b).

surface coverage of mild steel is expected. Similar results are obtained by Hassan [60] for corrosion inhibition of mild steel by triazole derivatives in HCl solution. Moreover, the values obtained for inhibitor **V** are lower than those obtained for inhibitor **I** in CO_2 containing brine which confirms that the inhibition efficiency of inhibitor V is slightly higher than that of inhibitor **I**. This behavior may be due to the slow rate of inhibitor adsorption with a resultant closer approach to equilibrium during the experiments at higher temperature [65]. One can conclude that, the decrease in activation energy with increasing additive concentration, in addition to the increase in $\eta\%$ in the presence of inhibitor with temperature, are suggestive of chemisorption of the inhibitor molecules on the metal surface [66].

3.9. Surface characterization

Fig. 16a shows an EDRF spectroscopy for mild steel surface. The characteristic peaks are related to the metals which are present in the alloy. In the absence of inhibitors, Fig. 17a exhibits the characteristic peaks which are related to Fe, Mn, P, Cr and oxygen elements. This indicated that the corrosion product on mild steel surface being metal oxide. However, the data in Figs. 18, 19a in the presence of 100 ppm of inhibitors **I** and **II** show additional peaks characteristic of Na and K elements, and the lower peaks height of Fe than those observed in the absence of inhibitors. This result proved that the adsorption of inhibitor molecule on mild steel surface leads to a decrease of metal oxide layer, and higher concentration of the inhibitor is necessary to delay the corrosion process.

Fig. 16b shows the SEM image of the mild steel surface. The micrograph shows the brightness of the electrode surface without any inclusions. Figs. 17–19b show SEM micrographs of the passive film formed on the mild steel surface after immersion in 1% NaCl saturated with CO_2 for 6 days in the absence and presence of inhibitors **I** and **II**. In the absence of inhibitors (Fig. 17b), the results exhibited that a thick porous layer of the corrosion product (oxide film) covered all electrode surfaces; the surface was strongly damaged, so that the electrode surface cannot be seen. Figs. 18, 19b show SEM of the electrode surface in the presence of 100 ppm of the inhibitors **I** and **II**. The micrographs revealed that, most of the electrode surface is covered by a protective layer and surface became free from damages and is smooth. This suggests that the inhibitor is strongly adsorbed on the mild steel surface, and this hinders the corrosion process and also confirms the highest inhibition efficiency of the prepared surfactants.

From quantitative analysis it can be observed that, there is a dramatic decrease in the thickness layer of iron over depth after the corrosion process in aggressive media without inhibitors, but in the presence of 100 ppm of inhibitors **I** and **II**, it is increased to 13.27 and 13.17 mm for inhibitors **I** and **II**, respectively. The quantitative analysis showed that, due to the presence of inhibitors in CO_2-saturated brine an adsorbed layer is formed on the metal surface, which successfully inhibits corrosion processes.

4. Conclusions

Weight loss, LPR corrosion rate, extrapolation of cathodic and anodic Tafel lines and surface tension methods were employed to study the corrosion inhibition of mild steel in CO_2-saturated 1% NaCl solution using some surfactants as corrosion inhibitors. The principal conclusions are:

1. The structures of synthesized surfactants were confirmed by physical–chemical spectroscopic methods and thermal analyses.
2. All studied surfactants were found to be effective inhibitors for mild steel corrosion in CO_2-saturated solutions.
3. The data obtained from all the used methods are in a good agreement with each other. The inhibition efficiency increased as both concentration of the inhibitor and temperature are increased.
4. The corrosion process is inhibited by the adsorption of these surfactants on mild steel surface. Inhibition efficiency was found to be in the following order: **V** > **IV** > **III** > **I** > **II**.
5. The adsorption of synthesized surfactants on mild steel surface obeyed the Langmuir adsorption isotherm. The values of the free energy for the adsorption process indicate that, the studied surfactants are chemically adsorbed on the metal surface.
6. The activation energy (E_a) decreases as inhibitor concentration increases. This can be explained as due to the enhancement of the inhibitor adsorption onto metal surface at higher temperatures.
7. SEM and EDRF observations of the electrode surface showed a good protective film present on the metal surface and also confirm the highest inhibition efficiency of the prepared surfactants.

Finally, all experimental results show that, the synthesized surfactants are good, safe and cheaper inhibitors for steel C1018 in CO_2 environments.

References

[1] G. Zhang, C. Chen, M. Lu, C. Chai, Y. Wu, Mater. Chem. Phys. 105 (2007) 331–340.
[2] R. De Marco, W. Durnie, A. Jefferson, B. Kinsella, A. Crawford, Corrosion 58 (2002) 354–363.
[3] P.C. Okafor, X. Liu, Y.G. Zheng, Corros. Sci. 51 (2009) 761–768.
[4] W.H. Durnie, B.J. Kinsella, R. De Marco, A. Jefferson, J. Appl. Electrochem. 31 (2001) 1221–1226.
[5] Qi Zhang, Zhinong Gao, Feng Xu, Xia Zou, Eng. Aspects 380 (2011) 191–200.
[6] G.Y. Elewady, I.A. El-Said, A.S. Fouda, Int. J. Electrochem. Sci. 3 (2008) 177–190.
[7] R. Fuchs-Godec, Colloids Surf. A 280 (2006) 130–139.
[8] R. Fuchs-Godec, V. Doleček, Colloids Surf. A 244 (2004) 73–76.
[9] R. Fuchs-Godec, Acta Chim. Slov. 54 (2007) 492–502.
[10] R. Fuchs-Godec, Electrochim. Acta 52 (2007) 4974–4981.
[11] R. Fuchs-Godec, Electrochim. Acta 54 (2009) 2171–2179.
[12] R. Fuchs-Godec, Ind. Eng. Chem. Res. 49 (2010) 6407–6415.
[13] N.A. Negm, F.M. Zaki, Colloids Surf. A 322 (2008) 97–102.
[14] X. Li, S. Deng, G. Mu, H. Fu, F. Yang, Corros. Sci. 50 (2008) 420–430.
[15] M.A. Hegazy, M.F. Zaky, Corros. Sci. 52 (2010) 1333–1341.
[16] B.N. Afanas'ev, Y.P. Akulova, Y.A. Polozhentseva, Prot. Met 44 (2) (2008) 134–140.
[17] M.M. Caroline, P. Christian, C.S. Hannes, K. Boris, A.A. Ilhan, Langmuir 24 (2008) 14269.
[18] A. Kumar, E-J. Chem. 5 (2008) 275–280.
[19] M.A. Malik, M.A. Hashim, F. Nabi, Sh.A. AL-Thabaiti, Z. Khan, Int. J. Electrochem. Sci. 6 (2011) 1927–1948.
[20] M.M. Osman, M.N. Shalaby, Mater. Chem. Phys. 77 (2002) 261–269.
[21] O. Olivares-Xometl, N.V. Likhanova, M.A. Domınguez-Aguilar, E. Arce, H. Dorantes, P. Arellanes-Lozada, Mater. Chem. Phys. 110 (2008) 344–351.
[22] G. Quartarone, M. Battilana, L. Bonaldo, T. Tortato, Corros. Sci. 50 (2008) 3467–3474.
[23] M.A. Amin, M.A. Ahmed, H.A. Arida, T. Arslan, M. Saracoglu, F. Kandemirli, Corros. Sci. 53 (2011) 540–548.
[24] M.P. Desimone, G. Gordillo, S.N. Simison, Corro. Sci. 53 (2011) 4033–4043.

[25] A. El-Sayed, H.S. Mohran, Hany M. Abd El-Lateef, J. Power Sources 196 (2011) 6573–6582.
[26] Alberta N.A. Aryee, Frederik R. Van de Voort, Benjamin K. Simpson, Process Biochem. 44 (2009) 401–405.
[27] T. Zhao, G. Mu, Corros. Sci. 41 (1997) 1937–1944.
[28] A. Singh, V.K. Singh, M.A. Quraishi, Rasayan J. Chem. 3 (4) (2010) 811–824.
[29] Y. Yan, L. Weihua, L. Cai, B. Hou, Electrochim. Acta 53 (2008) 5953–5960.
[30] M.A. Migahed, M. Abd-El-Raouf, A.M. Al-Sabagh, H.M. Abd-El-Bary, Electrochim. Acta 50 (2005) 4683–4689.
[31] N. Staicopolus, J. Electrochem. Soc. 110 (1963) 1121–1124.
[32] J. Crolet, N. Thevenot, S. Nesic, Corrosion 54 (1998) 194–203.
[33] K. Videm, J. Kvarekvaal, T. Perez, G. Fitzsimons, NACE Corrosion/96, Houston, Texas (1996), Paper No. 1.
[34] A. El-Sayed, A.M. Shaker, H.M. Abd El-Lateef, Corros. Sci. 52 (2010) 72–81.
[35] A.A. El-Shafei, S.A. Abd El-Maksoud, A.S. Fouda, Corros. Sci. 46 (2004) 579–590.
[36] R. Tremont, H. De Jesus-Cardona, J. Garcia-Orozco, R.J. Castro, C.R. Cabrera, J. Appl. Electrochem. 30 (2000) 737–743.
[37] J.W. Schultze, K. Wippermann, Electrochim. Acta 32 (1987) 823–831.
[38] M.S. Abdel Aal, A.A. Abdel Wahab, A. El-Sayed, Corrosion 37 (1981) 557–563.
[39] E. Akbarzadeh, M.N.M. Ibrahim, A.A. Rahim, Int. J. Electrochem. Sci. 6 (2011) 5396–5416.
[40] A. El-Sayed, Hossnia S. Mohran, H.M. Abd El-Lateef, Corros. Sci. 52 (2010) 1976–1984.
[41] D.A. López, S.N. Simison, S.R. de Sánchez, Corr. Sci. 47 (2005) 735–775.
[42] C. Cao, Corr. Sci. 38 (1996) 2073–2082.
[43] M. Nordsveen, S. Nesic, R. Nyborg, A. Stangelend, Corrosion 59 (2003) 443–456.
[44] F. Farelas, A. Ramirez, Int. J. Electrochem. Sci. 5 (2010) 797–814.
[45] Damián.A. López, S.N. Simison, S.R. de Sánchez, Electrochim. Acta 48 (2003) 845–854.
[46] G.I. Ogundele, W.E. White, Corrosion 42 (2) (1986) 71.
[47] J.K. Heuer, J.F. Stubbings, Corros. Sci. 41 (1999) 1231.
[48] M.J. Rosen, Surfactants and Interfacial Phenomena, 2nd ed., Wiley, New York, 1992.
[49] N.A. Negm, N.G. Kandile, I.A. Aiad, M.A. Mohammad, New eco-friendly cationic surfactants: Synthesis, characterization and applicability as corrosion inhibitors for carbon steel in 1 N HCl, Colloids Surf. A 391 (2011) 224–233.
[50] A.M. Al-Sabagh, N.M. Nasser, M.A. Migahed, N.G. Kandil, Egypt. J. Petrol. 20 (2011) 59–66.
[51] A.M. Badawi, M.A.S. Mohamed, M.Z. Mohamed, M.M. Khowdairy, J. Cancer Res. Ther. 3 (2007) 198–206.
[52] E.F. Moura, Alcides O.W. Neto, T.N.C. Dantas, H.S. Jnior, A. Gurgel, Colloids Surf. A 340 (2009) 199–207.
[53] W. Durnie, R. De Marco, A. Jefferson, B. Kinsella, J. Electrochem. Soc. 146 (1999) 1751–1756.
[54] M. Sahin, S. Bilgic, H. Yilmaz, Appl. Surf. Sci. 195 (2002) 1–7.
[55] R. Solmaz, G. Kardas, M. Culha, B. Yazici, M. Erbil, Electrochim. Acta 53 (2008) 5941.
[56] O. Olivares, N.V. Likhanova, B. Gomez, J. Navarrete, M.E. Llanos-Serrano, E. Arce, J.M. Hallen, Appl. Surf. Sci. 252 (2006) 2894–2909.
[57] S.A. Refay, F. Taha, A.M. Abd El-Malak, Appl. Surf. Sci. 236 (2004) 175–185.
[58] Z. Szklarska-Smialowska, J. Mankowski, Corros. Sci. 18 (1978) 953–960.
[59] A. Yurt, S. Ulutas, H. Dal, Appl. Surf. Sci. 253 (2006) 919–925.
[60] H.H. Hassan, Electrochim. Acta 53 (2007) 1722–1730.
[61] E.A. Noor, A.H. Al-Moubaraki, Mater. Chem. Phys. 110 (2008) 145–154.
[62] L. Herrag, B. Hammouti, S. Elkadiri, A. Aouniti, C. Jama, H. Vezin, F. Bentiss, Corros. Sci. 52 (2010) 3042–3051.
[63] M.A. Amin, S.S. Abd El-Rehim, E.E.F. El-Sherbini, R.S. Bayomi, Electrochim. Acta 52 (2007) 3588–3600.
[64] F. Bentiss, M. Lebrini, M. Lagrenee, Thermodynamic characterization of metal dissolution and inhibitor adsorption processes in mild steel/2,5-bis(n-thienyl)- 1,3,4 thiadiazoles/ hydrochloric acid system, Corros. Sci. 47 (2005) 2915–2931.
[65] S. Sankarapapavinasam, F.M. Ahmed, J. Appl. Electrochem. 22 (1992) 390.
[66] T.P. Hoar, R.D. Holliday, J. Appl. Chem. 3 (1953) 502–513.